Research Article

Received: 18 February 2011 Revised: 24 June 2011 Accepted: 27 June 2011 Published online in Wiley Online Library: 10 October 2011

(wileyonlinelibrary.com) DOI 10.1002/jsfa.4618

Stochastic state-space temperature regulation of biochar production. Part I: Theoretical development†

Keri B Cantrell* and Jerry H Martin II

Abstract

BACKGROUND: The concept of a designer biochar that targets the improvement of a specific soil property imposes the need for production processes to generate biochars with both high consistency and quality. These important production parameters can be affected by variations in process temperature that must be taken into account when controlling the pyrolysis of agricultural residues such as manures and other feedstocks.

RESULTS: A novel stochastic state-space temperature regulator was developed to accurately match biochar batch production to a defined temperature input schedule. This was accomplished by describing the system's state-space with five temperature variables – four directly measured and one change in temperature. Relationships were derived between the observed state and the desired, controlled state. When testing the unit at two different temperatures, the actual pyrolytic temperature was within 3 °C of the control with no overshoot.

CONCLUSION: This state-space regulator simultaneously controlled the indirect heat source and sample temperature by employing difficult-to-measure variables such as temperature stability in the description of the pyrolysis system's state-space. These attributes make a state-space controller an optimum control scheme for the production of a predictable, repeatable designer biochar.
Published 2011 by John Wiley & Sons, Ltd.

Keywords: pyrolysis; char; process control; waste treatment; waste minimization

INTRODUCTION

Slow pyrolysis of biomass is of special interest for the anoxic production of a solid product – char. Char is a relatively inert material useful as a soil amendment – a biochar – to improve crop yields and soil quality.[1–6] Just as the amount of biochar generated is dependent on both the type of feedstock and the maximum processing temperature, so the varying of process temperatures has been found to affect the way that biochars will react with soil/plant systems differently (see references cited in Ref. 4). Since different regions around the world have specific and individual soil quality issues, it follows that biochars could be designed or engineered to fit a specific need.[1] To ensure a biochar meets this need, a control system of substantially high quality is required to guarantee consistency in the biochar production processes. In doing so, the biochar product would have predictable and repeatable responses.

In the biochar literature it is commonplace to describe pyrolytic processes by specifying a temperature or temperature input schedule for a furnace (or other heat source); however, the actual temperature response of the feedstock during pyrolysis determines the biochar's characteristics. For larger-scale systems (e.g. bench, pilot and commercial scale), noticeable discrepancies can occur between the input temperature and actual temperature output; or in the case of biochar production the control temperature may not be the feedstock's exposure temperature. These variations in the feedstock's exposure temperature may be caused by process heat losses, process fatigue or deterioration, ambient temperature changes, feedstock loading methods and/or differences in the type of feedstock. Accounting for these instabilities is critical to the development of performance biochars. A process controller is needed that can exert precise control of the exposure temperature.

The large number of process instabilities renders classical control schemes impractical. An open-loop scheme takes far too long to reach the correct temperature, and there is no guarantee of accuracy. Traditional closed-loop schemes work for stable closed-loop systems, ideally allowing for elimination of offset, minimal disturbance effects, avoidance of excessive control action, rapid and smooth responses to setpoint changes, and robustness, making them insensitive to process conditions.[7] There are, however, inherent trade-offs, and not all ideals can be achieved with the control scheme. A conventional PID (proportional-integral-derivative) controller, as shown in Fig. 1, has an unavoidable trade-off between stability (tuning 1) and accuracy (tuning 2). Either choice will generate a biochar; however,

* *Correspondence to: Keri B Cantrell, USDA-ARS Coastal Plains Soil, Water & Plant Research Center, 2611 West Lucas Street, Florence, SC 29501-1241, USA. E-mail: keri.cantrell@ars.usda.gov*

USDA-ARS Coastal Plains Soil, Water & Plant Research Center, 2611 West Lucas Street, Florence, SC 29501-1241, USA

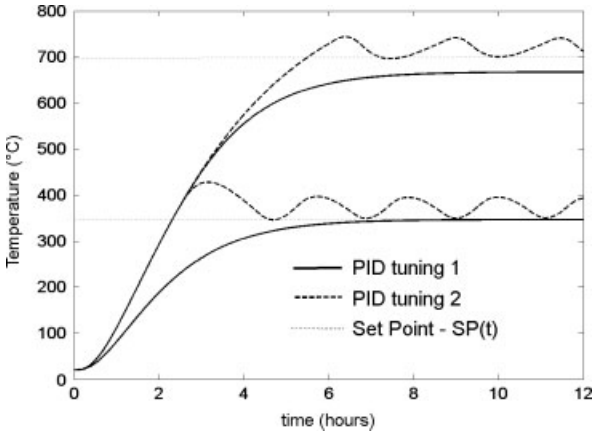

Figure 1. Simulated time *versus* temperature response to setpoints of 350 and 700 °C at PID tuning 1 (P = 1000, I = 1000, D = 100) and PID tuning 2 (P = 5, I = −6.9, D = 3.1).

the biochar properties may be either inconsistent or unique to the process equipment and conditions.

To generate a consistent, predictable biochar, the exposure temperature has to be both stable and accurate. A state-space regulator must be suitable for controlling systems that can be constantly affected by disturbances as well as multi-input/multi-output systems.[8] Previous state-space regulators were sometimes designed using a system model derived from physics; however, because of the high number of variables and the difficulty with quantifying how these variables are related, the state-space controller can use an empirical model with stochastic variables; thus, it would be a stochastic state-space regulator. Most state-space systems are represented using the following general form:

$$\dot{\boldsymbol{x}}(t) = \boldsymbol{A}\boldsymbol{x}(t) + \boldsymbol{B}\boldsymbol{u}(t) \quad (1)$$

$$\boldsymbol{y}(t) = \boldsymbol{C}\boldsymbol{x}(t) + \boldsymbol{D}\boldsymbol{u}(t) \quad (2)$$

In Eqn (1), $\boldsymbol{A}$ and $\boldsymbol{B}$ are system-descriptive, constant matrices, $\boldsymbol{x}(t)$ describes the system's state and $\boldsymbol{u}(t)$ is an input into an active element used to control the system (e.g. power input to a furnace). The concepts generalised by Eqn (2) are not needed to describe the controller, because there is no feedforward (i.e. $\boldsymbol{D} = 0$) and the system is digitally clocked. The digital clock cycle begins with the input state $\boldsymbol{x}(\boldsymbol{t})$ equalling the output of the last digital clock cycle, $\boldsymbol{y}(\boldsymbol{t})$; therefore $\boldsymbol{C}$ is unity. Thus Eqn (2) reduces to $\boldsymbol{y}(t) = \boldsymbol{x}(t)$. This implementation only uses Eqn (1).

The effects of instabilities in the system are mitigated by using knowledge of the system to derive observed values (Fig. 2). Observed values marked with a hat (^) are the output to a derived system of equations called the 'observer'. This has more in common with the knowledge of an experienced operator than directly measured values. Operators compare the difference – based on their knowledge and experience – between the desired and actual behaviour of the system before choosing the corrective course of action. The observer term achieves the same effect by using the coefficient $\boldsymbol{L}$ (Eqn (3)) to determine the correction to observed values based on the difference between the observed and measured values. In this way, knowledge of the system continuously mitigates the effect of unpredictable disturbances and instabilities.

$$\dot{\hat{\boldsymbol{x}}}(t) = \boldsymbol{A}\hat{\boldsymbol{x}}(t) + \boldsymbol{B}\boldsymbol{u}(t) + \boldsymbol{L}[\hat{\boldsymbol{x}}(t) - \boldsymbol{x}_{\text{measured}}(t)] \quad (3)$$

With the observer in place, the observed state $\hat{\boldsymbol{x}}(t)$ is continuously calculated by inputting knowledge of the state, along with its calculated derivative from the previous clock cycle (with a period Δt), into an integrator (Eqn (4)):

$$\hat{\boldsymbol{x}}(t) = \hat{\boldsymbol{x}}(t - \Delta t) + \int_{t-\Delta t}^{t} \dot{\hat{\boldsymbol{x}}}(t - \Delta t)\mathrm{d}t \quad (4)$$

The observed value is used to get the system to a desired state $\boldsymbol{x}_{\text{desired}}(t)$. To reach the desired state, the actual control mechanism uses the control matrix $\boldsymbol{K}$ to ascertain how much of an input applied to an open-loop reference input $\boldsymbol{r}(t)$ will cause the process to converge at $\boldsymbol{x}_{\text{desired}}(t)$ (Eqn (5)):

$$\boldsymbol{u}(t) = \boldsymbol{r}(t) + \boldsymbol{K}[\boldsymbol{x}_{\textbf{desired}}(t) - \hat{\boldsymbol{x}}(t)] \quad (5)$$

The desired state may be affected by multiple variables. These influences can easily be handled by a stochastic state-space controller (a true multi-input/multi-output controller). This is accomplished through the use of matrix variables. In the case of temperature-dependent processes such as pyrolytic production of biochar, including environmental variables such as surface and ambient temperatures (along with any other system variables such as pressure or mass flow rate[9,10]) in the state-space allows for this controller to achieve operation outside of a climate-controlled setting. With the addition of other system-descriptive temperatures such as the feedstock exposure temperature and the change in the heat source temperature in both $\hat{\boldsymbol{x}}(t)$ and $\boldsymbol{x}_{\text{desired}}(t)$, along with the selection of $\boldsymbol{K}$ so that both variables are controlled simultaneously, this regulator maintains simultaneous control of both the exposure temperature and stability of a heat source. The ability to heat feedstocks to a stable and accurate temperature with disturbance effects minimised (e.g. solar heating or convective cooling) means that the best control option for creating repeatable designer biochar is to employ a stochastic state-space regulator.

State-space theory in control design has been discussed in previous papers related to sterilisation of food products.[10–12] The application goal was comparable to that for designer biochar production in that better control of the sterilisation process both avoided undesirable degradation of nutrients and improved the quality of the final food product.[12] For biochar production, this would mean the avoidance of undesirable degradation of the feedstock in composition and structure to generate a consistent high-quality biochar. No design procedure has been documented for applying a stochastic state-space regulator to thermal processing of biomass to create high-quality designer biochars. Therefore this work sets out to develop a state-space regulator to accurately match the batch production of biochar to a defined temperature input schedule.

EXPERIMENTAL

Equipment selection

The original pyrolysis unit comprised a Lindburg electric box furnace equipped with a gas-tight retort (Model 51662, Lindburg/MPH, Riverside, MI, USA). The pyrolysis system was equipped with the following: gas cylinders containing zero-grade air (for cleaning) and industrial-grade N_2 (for pyrolysis) (items [7] and [8] respectively in Fig. 3); two Alcon 110VAC two-way solenoid valves (ITT, White Plains, NY, USA) (items [5] in Fig. 3); a 0–50 L min^{-1} gas flow controller (Model GFC37, Aalborg, Orangeburg, NY, USA)

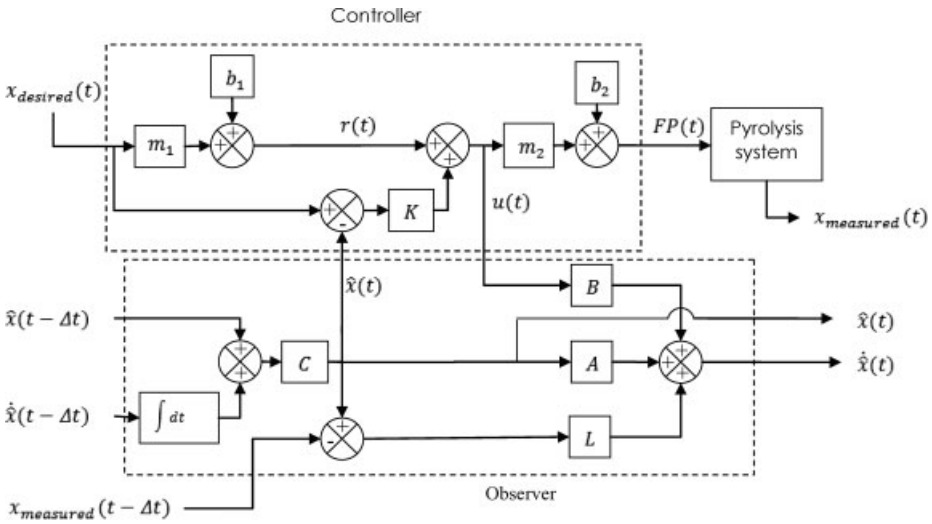

Figure 2. Block diagram of stochastic state-space regulator.

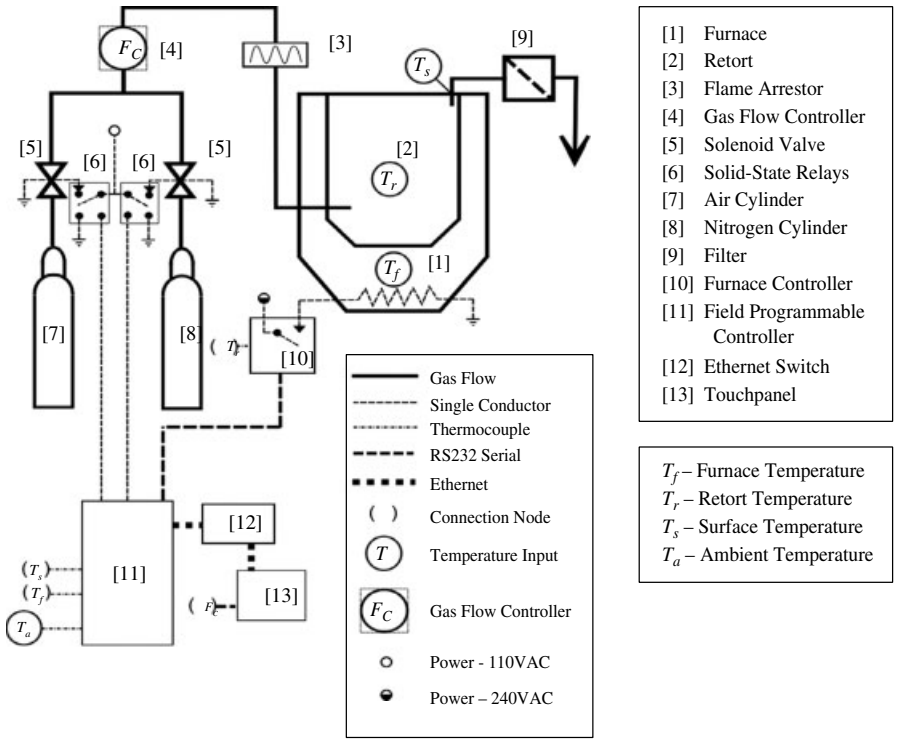

Figure 3. Pyrolysis system design with temperature inputs indicated.

(item [4] in Fig. 3); and a flame arrestor (item [3] in Fig. 3). The system was also equipped with a two-stage coalescing filter (Reading Technologies Inc., Reading, PA, USA) to remove impurities from the exhaust (item [9] in Fig. 3).

Original temperature control design

A PID controller (Eurotherm Model 2416, Ivensys, Ashburn, VA, USA) originally controlled the pyrolysis temperature using a single input signal from a thermocouple located near the furnace heating element. With the PID controller, either autotuned or tuned using Ziegler–Nichols rules,[13] it was found that control choices were limited to one of the following: (1) use a slow temperature ramp to avoid heat transfer limitations to the feedstock; (2) miss the desired response temperature over part of the temperature range; (3) allow the operator to correct a missed temperature; (4) allow an unstable response temperature to oscillate around the correct temperature; or (5) control the charring temperature from the wrong side of the retort boundary. Because any of those five choices could undesirably result in a slow reaction, the possibility of operator error, or arbitrary reaction temperatures when creating a designer char, the PID controller's usefulness was found to be quite limited.

In searching for a controller design without these limitations, it was decided to explore the furnace/retort's heating properties. The furnace/retort's existing controller was switched to open-loop (manual mode), allowing control of the power to the heating

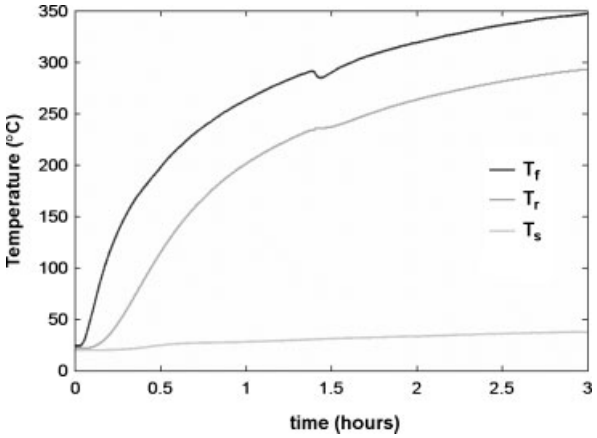

Figure 4. Pyrolysis system temperature response to a power input step of 24% (subscripts f = furnace, r = retort and s = retort surface).

element by varying the width of the electrical pulses – essentially a measure of the heating power – as a percentage. When a fixed power percentage was applied to a cool furnace, a lagging phenomenon was noted for the furnace/retort system: The furnace heated the fastest and achieved greater temperatures, followed by the retort heating more slowly to cooler temperatures, followed by the retort's surface heating very slowly to a much cooler temperature (Fig. 4). This occurred because heat propagated from the heating element in the furnace, through the walls of the retort and out from the surface of the retort. The temperature inside the retort, as opposed to the temperature of the furnace or surface, determined biochar characteristics directly (i.e. biochar's exposure temperature). Because of this, it was decided that the controller had to accurately control the retort's temperature. Controlling with only the retort temperature was difficult, because the properties of the heat propagation path were subject to variation, particularly from the rising surface temperature and variations in ambient temperature (e.g. morning *versus* midday temperatures). For these reasons, a regulator that could minimise the effect of the variation in thermal properties of the heat propagation path in the furnace/retort was chosen to control the charring reaction, which turned out to be a stochastic state-space regulator.

Modified set-up

The modified set-up retained the furnace and retort (items [1] and [2] respectively in Fig. 3), but features were added to allow a state-space regulator to control the retort's temperature response.

Control components

The state-space regulator was programmed into software written using Labview 2009 on a CompactRIO Model 9073 field programmable real-time controller available from National Instruments (Austin, TX, USA) and interfaced via a communications board (Eurotherm SUB24/EIA232) to the furnace's existing open-loop controller. The state of the furnace's heat propagation path was derived from multiple thermocouple measurements. These included: one located close to the heating element on the interior of the furnace ($\boldsymbol{T}_f$); a similar thermocouple inside a thermal well in the top-centre of the retort ($\boldsymbol{T}_r$); a type T thermocouple clamped to the retort's surface ($\boldsymbol{T}_s$); and another type T thermocouple measuring the ambient temperature ($\boldsymbol{T}_a$) (Fig. 3). These four temperatures, along with a user-selected pyrolysis method that included the input temperature schedule, were the main inputs used by the software driving the state-space temperature regulation of pyrolysis.

The heat propagation path's observed state

The state of the heat propagation path included multiple variables lumped together into an observed state vector $\hat{\boldsymbol{x}}(t)$ as shown in Eqn (6):

$$\hat{\boldsymbol{x}}(t)^T = [\dot{\hat{T}}_f(t)\hat{T}_f(t)\hat{T}_r(t)\hat{T}_s(t)\hat{T}_a(t)] \tag{6}$$

The state-space regulator regulated the open-loop furnace power $FP(t)$ so that the key metric in determining properties of the biochar – the retort temperature $T_r(t)$ – matched a schedule of input temperature setpoints $SP(t)$. The state-space regulator accomplished this by initialising the observer with measured temperature values and continuously solving Eqns (7)–(11) at each time t:

$$\hat{\boldsymbol{x}}(t) = \int_{t-\Delta t}^{t} \dot{\hat{x}}(t-\Delta t)dt = \hat{\boldsymbol{x}}(t-\Delta t) + \dot{\hat{x}}(t-\Delta t)\cdot\Delta t \tag{7}$$

$$\dot{\hat{x}}(t) = \boldsymbol{A}\hat{\boldsymbol{x}}(t) + \boldsymbol{B}\boldsymbol{u}(t) + \boldsymbol{L}[\hat{\boldsymbol{x}}(t) - \boldsymbol{x}_{\text{measured}}(t)] \tag{8}$$

$$\boldsymbol{u}(t) = \boldsymbol{r}(t) + \boldsymbol{K}[\boldsymbol{x}_{\text{desired}}(t) - \hat{\boldsymbol{x}}(t)] \tag{9}$$

$$\boldsymbol{r_1}(t) = f[SP(t)] = m1\cdot SP(t) + b1 \tag{10}$$

$$FP(t) = f[u(t)] = m2\cdot\boldsymbol{u_1}(t) + b2 \tag{11}$$

The derivation of the matrix constants was carried out with version R2008b of MATLAB (The MathWorks, Inc., Natick, MA, USA) using the long form of Eqns (7)–(9) as shown in Eqns (12)–(14):

$$\begin{bmatrix}\dot{\hat{T}}_f(t)\\ \hat{T}_f(t)\\ \hat{T}_r(t)\\ \hat{T}_s(t)\\ \hat{T}_a(t)\end{bmatrix} = \begin{bmatrix}\dot{\hat{T}}_f(t-\Delta t) + \ddot{\hat{T}}_f(t-\Delta t)\cdot\Delta t\\ \hat{T}_f(t-\Delta t) + \dot{\hat{T}}_f(t-\Delta t)\cdot\Delta t\\ \hat{T}_r(t-\Delta t) + \dot{\hat{T}}_r(t-\Delta t)\cdot\Delta t\\ \hat{T}_s(t-\Delta t) + \dot{\hat{T}}_s(t-\Delta t)\cdot\Delta t\\ \hat{T}_a(t-\Delta t) + \dot{\hat{T}}_a(t-\Delta t)\cdot\Delta t\end{bmatrix} \tag{12}$$

$$\begin{bmatrix}\ddot{\hat{T}}_f(t)\\ \dot{\hat{T}}_f(t)\\ \dot{\hat{T}}_r(t)\\ \dot{\hat{T}}_s(t)\\ \dot{\hat{T}}_a(t)\end{bmatrix} = \begin{bmatrix}a_{11} & a_{12} & 0 & 0 & 0\\ 1 & 0 & 0 & 0 & 0\\ 0 & a_{32} & a_{33} & a_{34} & 0\\ 0 & 0 & a_{43} & a_{44} & a_{45}\\ 0 & 0 & 0 & 0 & 0\end{bmatrix}$$

$$\begin{bmatrix}\dot{\hat{T}}_f(t)\\ \hat{T}_f(t)\\ \hat{T}_r(t)\\ \hat{T}_s(t)\\ \hat{T}_a(t)\end{bmatrix} = \begin{bmatrix}1\\0\\0\\0\\0\end{bmatrix}[u_1(t)\quad 0\quad 0\quad 0\quad 0] +$$

$$\begin{bmatrix}l_{\dot{T}_f} & 0 & 0 & 0 & 0\\ 0 & l_{T_f} & 0 & 0 & 0\\ 0 & 0 & l_{T_r} & 0 & 0\\ 0 & 0 & 0 & l_{T_s} & 0\\ 0 & 0 & 0 & 0 & 1\end{bmatrix}\begin{bmatrix}\dot{T}_f(t) - \dot{\hat{T}}_f(t)\\ T_f(t) - \hat{T}_f(t)\\ T_r(t) - \hat{T}_r(t)\\ T_s(t) - \hat{T}_s(t)\\ T_a(t) - \hat{T}_a(t)\end{bmatrix} \tag{13}$$

$$\boldsymbol{u_1}(t) = \boldsymbol{r_1}(t) + \boldsymbol{k_{T_r}}\cdot\boldsymbol{SP}(t) - [k_{\dot{T}_f}\quad 0\quad k_{T_r}\quad 0\quad 0]$$
$$[\dot{\hat{T}}_f(t)\quad \hat{T}_f(t)\quad \hat{T}_r(t)\quad \hat{T}_s(t)\quad \hat{T}_a(t)]^T \tag{14}$$

RESULTS AND DISCUSSION

Development of the stochastic state-space regulator

Deriving the variables for the regulator using six basic system conditions

The variables for the stochastic state-space regulator were derived by amalgamating assumptions to create differing conditions in

Table 1. Six conditions within a state-space of a furnace/retort pyrolysis system

Condition	Assumption	Effect	Regulator
Steady-state	$t \gg t_0$ $\dot{\boldsymbol{x}}(t) \approx 0$	Quasi-thermal equilibrium	$\boldsymbol{x}(t) \approx \boldsymbol{x}_\infty$ $\dot{\boldsymbol{x}}(t) \approx 0$
De-energised	$\boldsymbol{u}(t) = 0$	No control terms	$\dot{\boldsymbol{x}}(t) = \boldsymbol{A}\hat{\boldsymbol{x}}(t) + \boldsymbol{L}[\hat{\boldsymbol{x}}(t) - \boldsymbol{x}_{\mathbf{measured}}(t)]$
Open-loop	$\boldsymbol{K} = 0$ $\boldsymbol{u}(t) = \boldsymbol{r}(t)$	No feedback (closed-loop) terms	$\dot{\boldsymbol{x}}(t) = \boldsymbol{A}\hat{\boldsymbol{x}}(t) + \boldsymbol{B}\boldsymbol{r}(t) + \boldsymbol{L}[\hat{\boldsymbol{x}}(t) - \boldsymbol{x}_{\mathbf{measured}}(t)]$
Amaurotic	$\hat{\boldsymbol{x}}(t) = \boldsymbol{x}_{\mathbf{measured}}(t)$	Observed values are measured values	$\dot{\boldsymbol{x}}(t) = \boldsymbol{A}\boldsymbol{x}_{\mathbf{measured}}(t) + \boldsymbol{B}\boldsymbol{u}(t)$ $\boldsymbol{u}(t) = \boldsymbol{r}(t) + \boldsymbol{K}[\boldsymbol{x}_{\mathbf{desired}}(t) - \boldsymbol{x}_{\mathbf{measured}}(t)]$
Purblind	$\boldsymbol{L} = 0$	Measured values have no effect	$\dot{\boldsymbol{x}}(t) = \boldsymbol{A}\hat{\boldsymbol{x}}(t) + \boldsymbol{B}\boldsymbol{u}(t)$ $\boldsymbol{u}(t) = \boldsymbol{r}(t) + \boldsymbol{K}[\boldsymbol{x}_{\mathbf{desired}}(t) - \boldsymbol{x}(t)]$
Desired	$\hat{\boldsymbol{x}}(t) = \hat{\boldsymbol{x}}_{\mathbf{desired}}(t)$ $\hat{\boldsymbol{x}}(t) = \hat{\boldsymbol{x}}_{\mathbf{measured}}(t)$	Steady-state system behaviour goal	$\dot{\boldsymbol{x}}(t) = \boldsymbol{A}\hat{\boldsymbol{x}}(t) + \boldsymbol{B}\boldsymbol{u}(t) + \boldsymbol{L}[\hat{\boldsymbol{x}}(t) - \boldsymbol{x}_{\mathbf{measured}}(t)]$ $\boldsymbol{u}(t) = \boldsymbol{r}(t) + \boldsymbol{K}[\boldsymbol{x}_{\mathbf{desired}}(t) - \hat{\boldsymbol{x}}(t)]$

the furnace/retort's heat propagation path (Table 1) useful for mathematically isolating and deriving variables in the state-space regulator. The six conditions were the following: (1) the steady-state condition (thermal quasi-equilibrium approached over an extended period of time); (2) the de-energised condition (no power input, thus no control term $\boldsymbol{u}$(t)); (3) the open-loop condition (no feedback, thus $\boldsymbol{K} = 0$); (4) the amaurotic condition (the observer is blinded so that only measured values affect the regulator); (5) the purblind condition (the observer is blinded so that measured values have no effect on the regulator, i.e. $\boldsymbol{L} = 0$); and finally (6) the desired condition (when the measured state equals the desired state). Knowledge of how these conditions affect the behaviour of the heat propagation path was key to deriving a regulator capable of driving the retort's temperature through the stochastic state-space describing the heat propagation path to the desired temperature that would result in the production of biochar with consistent and controlled properties.

*Deriving the system matrix (**A**) by amaurotic observation of the de-energised cooling of the heat propagation path*

The ***A*** matrix constant was used to describe the temperature properties of the heat propagation path. By using amaurotic observation (which is conceptually similar to using direct measurement) of the cooling, de-energised heat propagation path, the ***A*** matrix could be determined. The term amaurotic (normally used to describe a type of blindness when the eyes function but do not see) was used to describe a regulator that uses sensor inputs but does not observe. By using amaurotic observation, the measured value was set equal to the observed value, and by using de-energised cooling, the control term $\boldsymbol{u}(t)$ drops out of Eqn (8), simplifying it to Eqn (15):

$$\dot{\boldsymbol{x}}_{\mathbf{measured}}(t) = \boldsymbol{A}\boldsymbol{x}_{\mathbf{measured}}(t) \tag{15}$$

The ***A*** matrix was derived from temperature values obtained by cooling the furnace/retort from a heated thermal equilibrium (an initial, open-loop condition of $\boldsymbol{T}_r = 800\,^\circ\mathrm{C}$ with $\boldsymbol{FP} = 90\%$) to a cooled thermal equilibrium (a steady-state, de-energised condition). The ***A*** matrix was a selection of stochastic variables – a stochastic state-space – only loosely resembling differential equations used to describe a deterministic model of heat propagating from the heating element through the sample to the ambient environment (Eqns (16)–(20)); the relations were chosen and then regressed as shown in Fig. 5 to derive the values for the ***A*** constant.

$$\ddot{\boldsymbol{T}}_f/\boldsymbol{T}_f = a_{11}(\dot{\boldsymbol{T}}_f/\boldsymbol{T}_f) + a_{12} \tag{16}$$

$$\boldsymbol{0} = a_{32} + a_{33} + a_{34} \tag{17}$$

$$\dot{\boldsymbol{T}}_r/(\boldsymbol{T}_s - \boldsymbol{T}_f) = a_{33}[(\boldsymbol{T}_r - \boldsymbol{T}_f)/(\boldsymbol{T}_s - \boldsymbol{T}_f)] + a_{34} \tag{18}$$

$$\boldsymbol{0} = a_{43} + a_{44} + a_{45} \tag{19}$$

$$\dot{\boldsymbol{T}}_s/(\boldsymbol{T}_a - \boldsymbol{T}_r) = a_{44}[(\boldsymbol{T}_s - \boldsymbol{T}_r)/(\boldsymbol{T}_a - \boldsymbol{T}_r)] + a_{45} \tag{20}$$

*Deriving the **B** matrix*

The ***B*** matrix described the effect of energising the heating element. Since there was only one heating element located in the furnace, energising the element only affected how much the temperature of the furnace changed; $\boldsymbol{B}^T$ was $[1 \quad 0 \quad 0 \quad 0 \quad 0]$.

The relationship between the control vector $\boldsymbol{u}(t)$ and the reference vector r(t)

The control vector $\boldsymbol{u}(t)$, or in this case $[u_1 \quad 0 \quad 0 \quad 0 \quad 0]$, determined how much the energising of the heating element affected the propagation path. In an open-loop condition, there was no control, so the feedback term ***K*** was set to 0 and the control value was fixed at the reference value; hence, when operating in open-loop, $\boldsymbol{u}(t) = \boldsymbol{r}(t)$. In this case, $\boldsymbol{r}$(t) equalled $[r_1 \quad 0 \quad 0 \quad 0 \quad 0]$.

*Deriving the relationship between the reference vector **r**(t) and the setpoint SP(t) by purblind observation of open-loop warming of the heat propagation path*

The setpoint temperature $SP(t)$ was the desired temperature of the retort. By using purblind observation (which was conceptually similar to using a mathematical model) of the open-loop warming of the heat propagation path, the different reference values $\boldsymbol{r}(t)$ could be correlated with different potential setpoints. The term purblind (normally used to describe a type of blindness when the eyes do not function and cannot see) was used to describe a regulator that does not observe. By using a purblind regulator, the ***L*** term was set to 0, whence Eqn (8) became Eqn (21):

$$\dot{\boldsymbol{x}}(t) = \boldsymbol{A}\boldsymbol{x}(t) + \boldsymbol{B}\boldsymbol{r}(t) \tag{21}$$

Equation (21), along with the previously derived ***A*** matrix, was used to determine the quasi-equilibrium temperatures of the propagation path given different reference values $\boldsymbol{r}(t)$. Since quasi-equilibrium retort temperature values could be used as potential setpoints, this information was used to derive the relationship between the reference vectors $\boldsymbol{r}(t)$ and different potential $SP(t)$ and eventually used to derive $m1$ and $b1$ in Eqn (10).

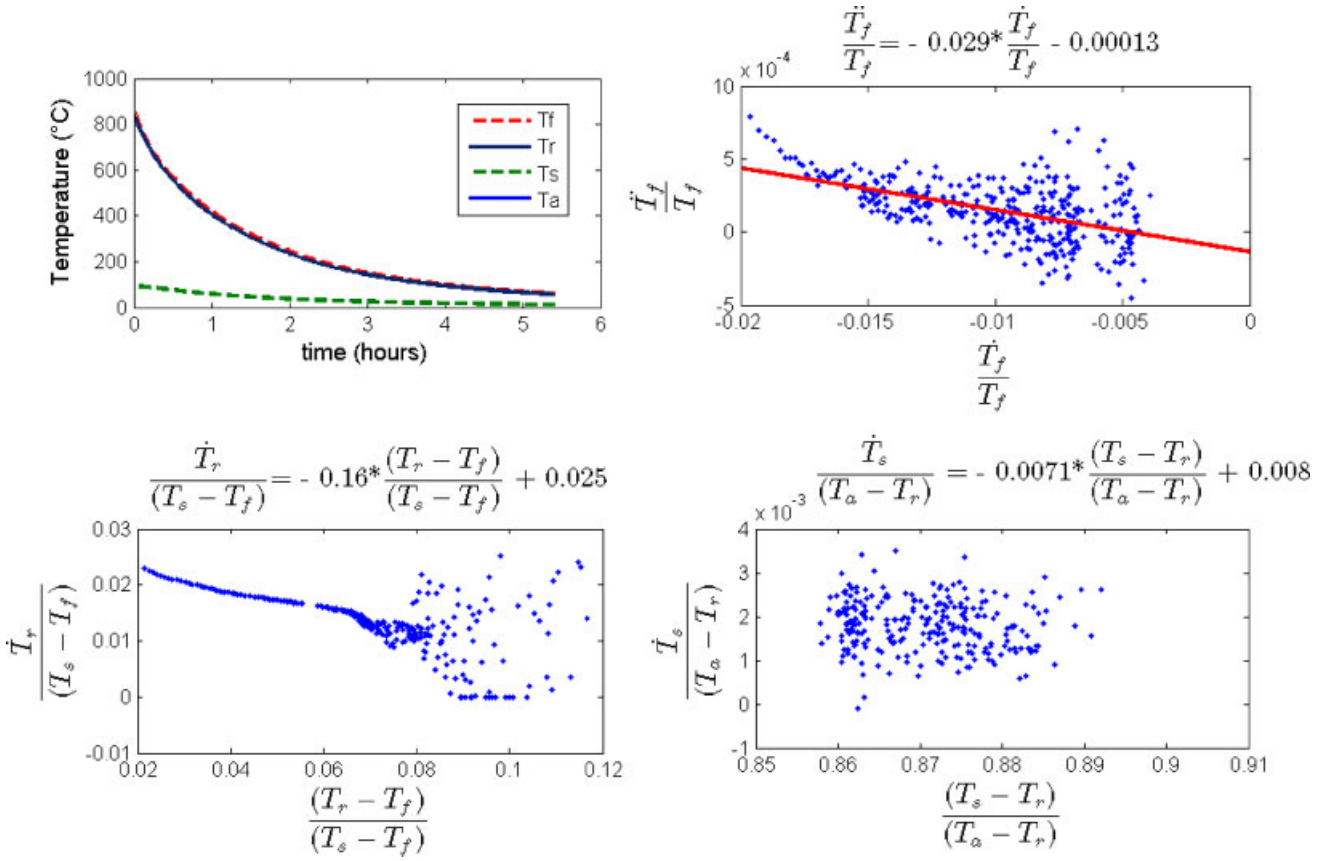

Figure 5. Derivation of ***A*** matrix: top-left, data used for derivation; top-right, derivation of a_{11} and a_{12}; bottom-left, derivation of a_{33} and a_{34}; bottom-right, derivation of a_{44} and a_{45}.

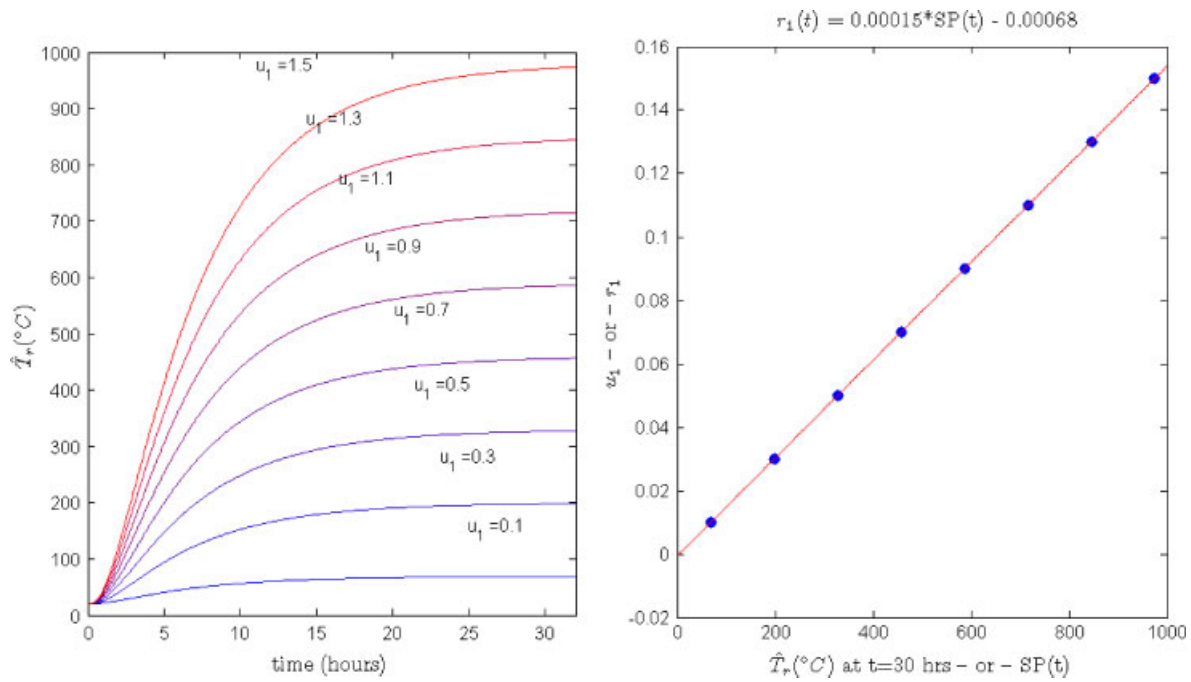

Figure 6. Derivation of *m1* and *b1* parameters.

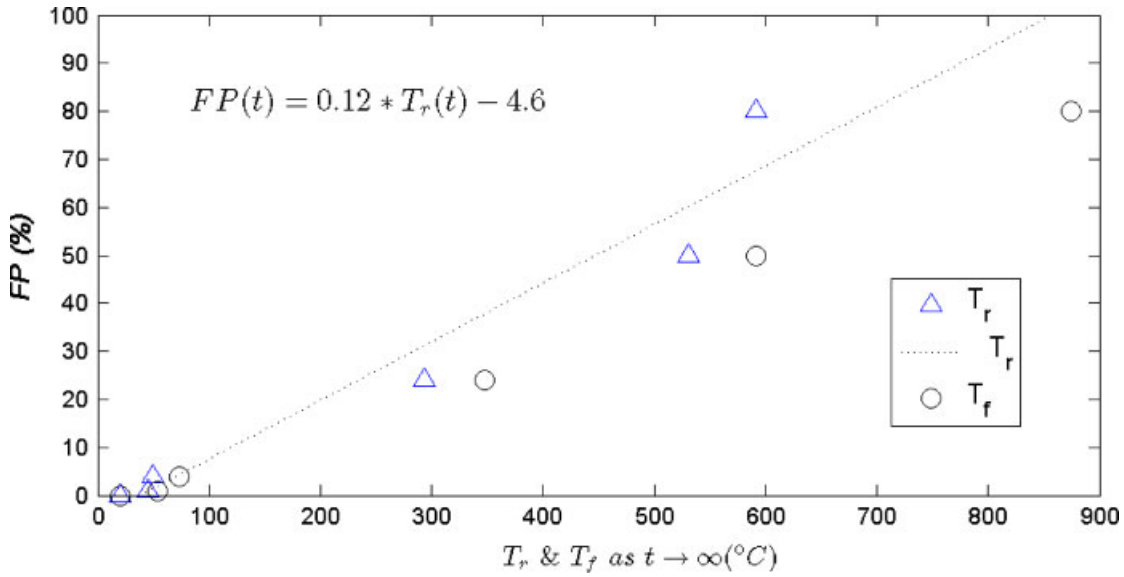

Figure 7. Open-loop power output as a function of desired temperatures.

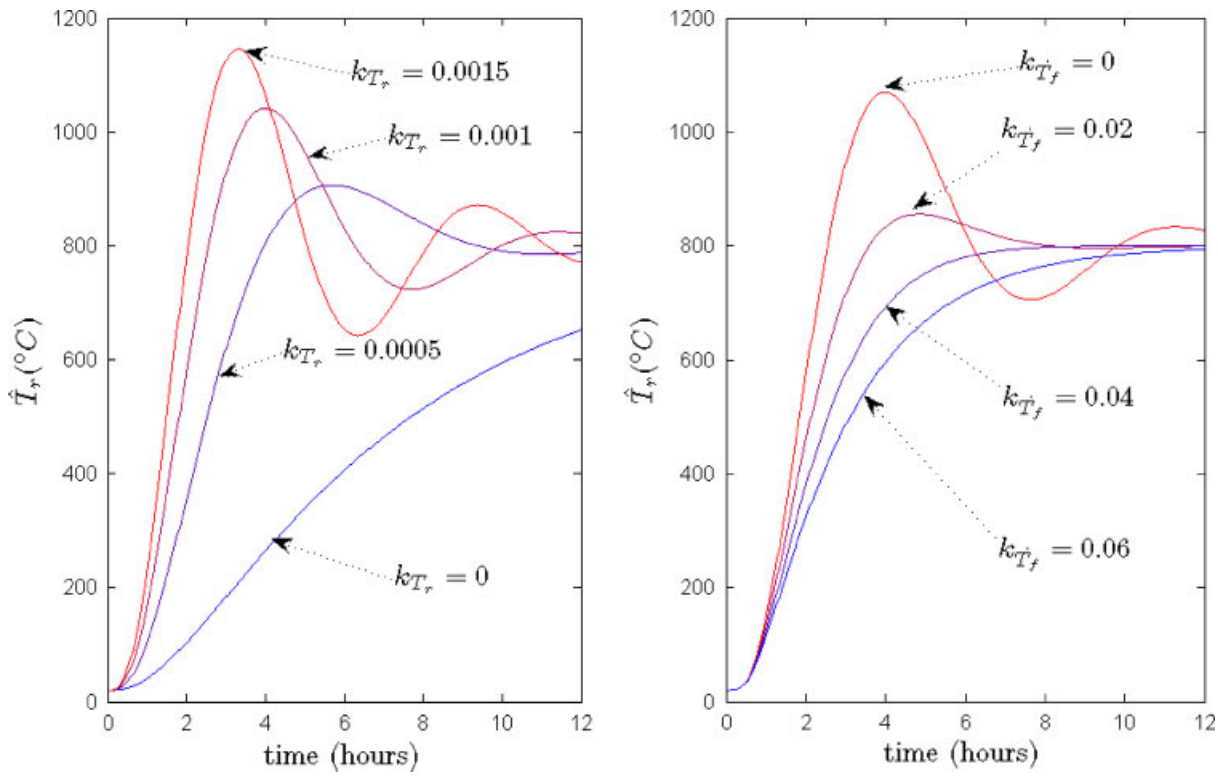

Figure 8. Derivation of k_{T_r} (left) and derivation of k_1 at $k_{T_r} = 0.001$ (right) simulated as response to a step input of ***SP*** = 800 °C.

*Deriving the relationship between the control vector **u**(t) and the furnace power **FP**(t) by purblind and amaurotic observation of open-loop warming of the heat propagation path*

The relationship between ***u***(*t*) (which was equivalent to ***r***(*t*) in open-loop) and ***FP***(t) was derived using the previously determined quasi-equilibrium temperatures of the propagation path given different reference values ***r***(*t*), and by amaurotic observation of quasi-equilibrium temperatures using actual open-loop values of the furnace power ***FP***(*t*) (Fig. 6). From this information, a regression determining the relationship between ***FP***(*t*) and ***u***(*t*) in Eqn (22) was used to derive *m*2 and *b*2 in Eqn (11) (Fig. 7):

$$FP(t) = m2 \cdot m1 \cdot \lim_{dT/dt \to 1^\circ C/10\ min} T_r(t) + (m2 \cdot b1 + b2) \quad (22)$$

*Deriving the **K** value to drive the purblind regulator to the desired setpoint **SP**(t)*

A purblind regulator consisting of Eqns (8) and (9) was used to select an ideal ***K*** value by testing the ability of different ***K*** matrices to bring the retort temperature to a desired state. The desired state (Eqn (23)) was to not only accurately follow *SP*(*t*) with $\hat{T}_r(t)$ but to

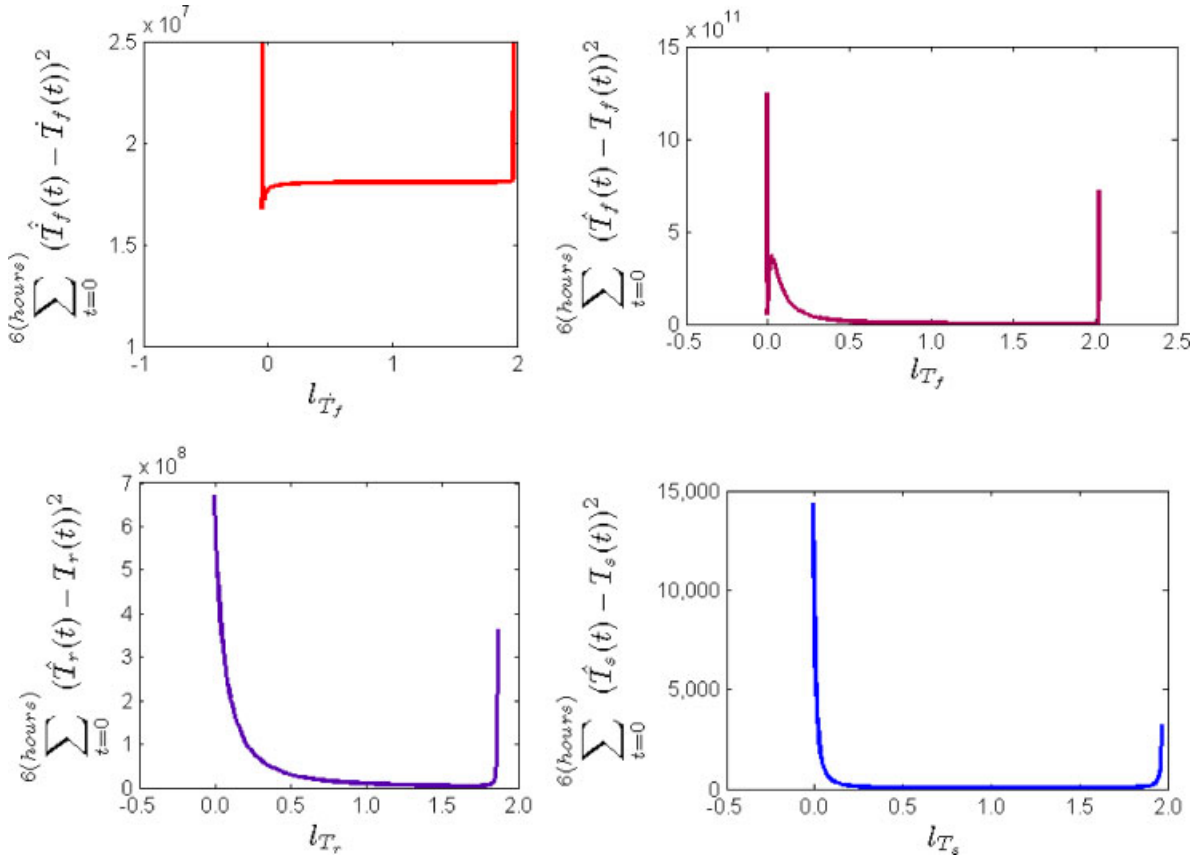

Figure 9. Sum of squares of error between actual temperature and measured temperature for each *l* value for each temperature.

also stabilise the furnace temperature (i.e. $\dot{\hat{T}}_f(t) = 0$), which had to be maintained at an unpredictably higher temperature than *SP*(*t*). The ***K*** matrices were tested (Eqn (5)) and the k_{T_r} value was selected to give the controller a strong tendency to pull $\hat{\boldsymbol{T}}_r(\boldsymbol{t})$ to the desired temperature. Additionally, the $k_{\dot{T}_f}$ term was selected to give the controller a weak tendency to stabilise the change in furnace temperature. Among the two controller terms, the k_{T_r} term was selected first with a value of 0.001; this term was intentionally chosen to be unstable – notice the large temperature overshoot in Fig. 8 – to give the retort a fast response time. The next term selected was the $k_{\dot{T}_f}$ term; this term was selected at a value of 0.04 to minimise the overshoot while maintaining the fast response time.

$$\boldsymbol{x}_{\text{desired}}(t)^{\mathrm{T}} = [\,0 \quad 0 \quad SP(t) \quad 0 \quad 0\,] \tag{23}$$

$$\boldsymbol{K} = [\,k_{\dot{T}_f} \quad 0 \quad k_{T_r} \quad 0 \quad 0\,] \tag{24}$$

*Deriving the **L** matrix by observation of the de-energised cooling of the heat propagation path*

The ***L*** matrix determined which point between amaurotic and purblind observation values was appropriate for each value used in operating the regulator. This was advantageous because $\dot{\hat{T}}_f(t)$ was difficult to measure, thus purblind observation was better, while $\boldsymbol{T}_a$ was impossible to predict, so amaurotic observation was more appropriate. A series of ***L*** matrix values (except for l_a, which was always unity) was tested to see which value minimised the sum of the square of the error between the observed and actual values while observing the cooling of a de-energised heat propagation path. Figure 9 demonstrates the effect of different *l* terms when either the purblind observer ($\boldsymbol{l} \to -\infty$) or the amaurotic observer ($\boldsymbol{l} \to \infty$) was allowed influence over the control. By using an observer that could strike a balance between amaurotic and purblind observation (using both measured and predicted values) of the heat propagation path as a basis for feedback control, any effects caused by variations in the heat propagation path could be minimised.

Regulating to the desired temperature of biochar

For the current pyrolysis system, the stochastic state-space regulator was designed to (1) use multiple temperature variables to regulate the state of the heat propagation path, (2) control the retort temperature while stabilising the furnace temperature at an unpredictably higher level and (3) minimise the effects of variation in the heat propagation path by using an observed state. With these properties the stochastic state-space regulator pyrolysed biomass to a stable version of the desired temperature response (Fig. 10).

For two different maximum exposure temperature profiles tested, one at 350 °C and the other at 700 °C, the state-space controller was able to accurately control the desired pyrolysis temperature (i.e. T_r). Within 15 min the temperature within the retort achieved the initial 200 °C condition. Within 30 min the temperature within the retort was stable around 200 °C. For the 2.5 °C min^{-1} ramp to 350 °C, the regulator was able to control the retort temperature to within 5 °C of T_{desired}. For the 8.33 °C min^{-1} ramp to 700 °C, some lag in temperature occurred after 600 °C as heat propagated through the system, as noted by an increase in

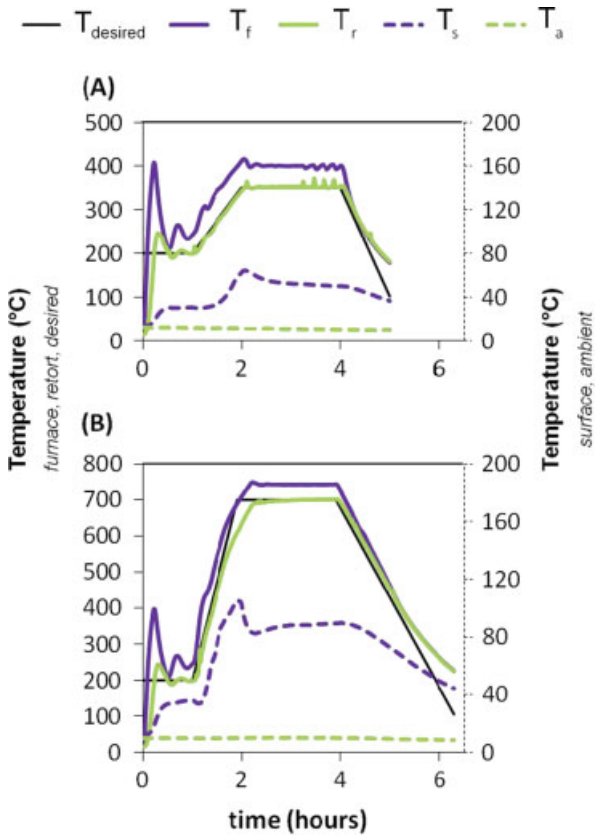

Figure 10. Temperature responses during stochastic state-space temperature regulation of pyrolysis system at (A) 350 and (B) 700 °C.

T_s. However, T_r was equivalent to $T_{desired}$ within 30 min with no overshoot. The regulator was able to control T_r during a majority of the cooling phase of the pyrolysis run until the system reached a de-energised condition. In both instances, once maximum exposure temperature was achieved, the controller maintained T_r to within 3 °C of $T_{desired}$. Evaluation of individual physical and compositional characteristics of the biochars is presented in Part II.[14]

CONCLUSION

Following the concept that biochars need to be designed to target a specific soil need, process controls for the pyrolysis process need to be developed that guarantee consistent and high-quality biochar production. State-of-the-art control must compensate for temperature variations (e.g. due to chemical or physical anomalies) and ensure that the feedstock is being pyrolysed according to the specified input temperature schedule. A stochastic state-space regulator was successfully developed for a batch, furnace/retort pyrolysis system that (1) used multiple temperatures to regulate the state of the heat propagation path, (2) controlled the retort temperature while stabilising the furnace temperature at an unpredictably higher level and (3) minimised the effects of variation in the heat propagation path by using the observed state. These attributes made the state-space regulator an optimal choice for biochar production.

ACKNOWLEDGEMENT

Mention of a trade name, proprietary product or vendor is for information only and does not guarantee or warrant the product by the USDA and does not imply its approval to the exclusion of other products or vendors that may also be suitable.

REFERENCES

1 Novak JM, Lima I, Baoshan X, Gaskin JW, Steiner C, Das KC, *et al*, Characterization of designer biochar produced at different temperatures and their effects on a loamy sand. *Ann Environ Sci* **3**:195–206 (2009).
2 Glaser B, Lehmann J and Zech W, Ameliorating physical and chemical properties of highly weathered soils in the tropics with charcoal – a review. *Biol Fertil Soils* **35**:219–230 (2002).
3 Novak JM, Busscher WJ, Laird DL, Ahmedna M, Watts DW and Niandou MAS, Impact of biochar amendment on fertility of a southeastern coastal plain soil. *Soil Sci* **174**:105–112 (2009).
4 Chan KY and Xu Z, Biochar: nutrient properties and their enhancement, in *Biochar for Environmental Management: Science and Technology*, ed. by Lehmann J and Joseph S. Earthscan, Sterling, VA, pp. 67–84 (2009).
5 Roberts KG, Gloy BA, Joseph S, Scott NR and Lehmann J, Life cycle assessment of biochar systems: estimating the energetic, economic, and climate change potential. *Environ Sci Technol* **44**:827–833 (2010).
6 Sohi S, Lopez-Capel E, Krull E and Bol R, Biochar, climate change and soil: a review to guide future research. *CSIRO Land and Water Science Report 05–09*, CSIRO Land and Water, Australia (2009).
7 Seborg DE, Edgar TF and Mellichamp DA, *Process Dynamics and Control*. Wiley, New York, NY (1989).
8 Lewis FL, *Applied Optimal Control and Estimation: Digital Design &Implementation*. Prentice-Hall, Upper Saddle River, NJ (1992).
9 Luenberger DG, Observers for multivariable systems. *IEEE Trans Automat Control* **AC-11**:190–197 (1966).
10 Mulvaney SJ, Rizvi SSH and Johnson JCR, Dynamic modeling and computer control of a retort for thermal processing. *J Food Eng* **11**:273–289 (1990).
11 Alonso AA, Banga JR and Perez-Martin R, A complete dynamic model for the thermal processing of bioproducts in batch units and its application to controller design. *Chem Eng Sci* **52**:1307–1322 (1997).
12 Alonso AA, Banga JR and Perez-Martin R, Modeling and adaptive control for batch sterilization. *Comput Chem Eng* **22**:445–458 (1998).
13 Ogata K, *Modern Control Engineering*. Prentice Hall, Upper Saddle River, NJ (2002).
14 Cantrell KB and Martin II JH, Stochastic state-space temperature regulation of biochar production. Part II: Application to manure processing pyrolysis. *J Sci Food Agric* **00**:000–000 (2011).